crystals

MDPI

Article

Scintillation Properties of Pr-Doped Lanthanum Pyrosilicate Single Crystals

Prom Kantuptim, Takumi Kato, Daisuke Nakauchi, Noriaki Kawaguchi and Takayuki Yanagida *

Division of Materials Science, Graduate School of Science and Technology, Nara Institute of Science and Technology, 8916-5 Takayama, Ikoma 630-0192, Nara, Japan; prom.kantuptim.pf2@ms.naist.jp (P.K.); kato.takumi.ki5@ms.naist.jp (T.K.); nakauchi@ms.naist.jp (D.N.); n-kawaguchi@ms.naist.jp (N.K.)
* Correspondence: t-yanagida@ms.naist.jp

Abstract: Five samples of lanthanum pyrosilicate ($La_2Si_2O_7$) single crystals with 0.5–10.0% Praseodymium (Pr)-doping concentrations were synthesized by the floating-zone method. Photoluminescence and scintillation properties of these crystals were investigated in this study for the first time. The multiple emissions from electron transitions of Pr^{3+} were observed on both a photoluminescence emission map and scintillation spectra, including the desired emission band of Pr^{3+} 5d–4f transition at 250–310 nm. The major photoluminescence and scintillation decay times were approximately 19 and 26 ns, respectively. When compared with commercial scintillators such as Tl-doped cesium iodide (CsI), the Pr-doped $La_2Si_2O_7$ samples presented a respectively low afterglow level of 32 ppm after 20 ms of X-ray irradiation. Under 662 keV γ-ray irradiation from ^{137}Cs, the 3.0% Pr-doped $La_2Si_2O_7$ sample presented a scintillation light yield of 3200 ph/MeV, which was the best value among the tested samples.

Keywords: lanthanum pyrosilicate; Pr^{3+}; photoluminescence; scintillator

Citation: Kantuptim, P.; Kato, T.; Nakauchi, D.; Kawaguchi, N.; Yanagida, T. Scintillation Properties of Pr-Doped Lanthanum Pyrosilicate Single Crystals. *Crystals* **2022**, *12*, 459. https://doi.org/10.3390/cryst12040459

Academic Editors: Fu-Der Lai, Mu-Chun Wang and Wen-Ching Hsieh

Received: 28 February 2022
Accepted: 22 March 2022
Published: 25 March 2022

1. Introduction

Ionizing radiation has become one of the useful tools that benefit human life. From the middle of the 20th century to the present, both academia and industry have made an effort to use ionizing radiation more efficiently and accurately for their research, products, and services. To obtain the benefits of ionizing radiation properly, detection and measurement systems are necessary. A scintillator is a special category of phosphor material that has a very unique ability to convert ionizing radiation such as X- and γ-rays to lower energy photons such as ultraviolet and visible light [1,2]. In particular, the solid scintillators come in many forms of materials, including plastics [3,4], glass [5–7], transparent ceramics [8,9], inorganic–organic perovskite [10,11], and single crystals [12–14]. Generally, these scintillators are combined with photodetectors such as photomultiplier tubes, silicon photomultipliers (SiPMs), or photodiodes. Such sensors are called scintillation detectors. To date, scintillation detectors have been used in many kinds of professional applications such as astrophysics [15], geophysics [16], border security [17], environmental observation [18], natural resource exploration [19], and many more.

A fast scintillator has become essential to the development of high-detection rate detectors for positron emission tomography (PET) [20,21]. The trivalent praseodymium ion (Pr^{3+})-activated scintillators have an advantage in this field since they show the fast scintillation decay time of ~20 ns due to 5d–4f transitions of Pr^{3+}. An example is the Pr-doped lutetium aluminum garnet ($Lu_3Al_5O_{12}$, LuAG) which is used for the abovementioned PET scanner for breast cancer imaging [22]. In terms of the host materials, pyrosilicate materials ($X_2Si_2O_7$, where X is rare earth) are becoming one of the potential candidates for novel high-performance scintillators. One of the famous materials in this group is the Ce-doped lutetium pyrosilicate ($Lu_2Si_2O_7$, LPS) with a high scintillation light yield of 26,300 ph/MeV and a fast decay time of 38 ns [23]. Following the study on Ce-doped LPS,

we have investigated Pr-doped LPS, gadolinium pyrosilicate ($Gd_2Si_2O_7$, GPS), and yttrium pyrosilicate ($Y_2Si_2O_7$, YPS) and successfully observed 5d–4f transitions of Pr^{3+} [24–26].

Lanthanum pyrosilicate ($La_2Si_2O_7$, LaPS) is one of the pyrosilicate group materials. In a recent study, when doped with Ce, the LaPS showed interesting scintillation characteristics such as a medium scintillation light yield of 5400 ph/MeV with low afterglow of 30 ppm and fast scintillation decay time of 26 ns [27]. The combination of the newly discovered LaPS host with the fast Pr^{3+} is expected to deliver interesting scintillation properties in both fast decay time and high scintillation light yield. This study is the first attempt to use Pr^{3+} as a luminescence center in the LaPS single-crystal host. The characterizations of Pr-doped LaPS are covered by both photoluminescence (PL) and scintillation properties, including PL emission spectrum, PL decay time, scintillation spectrum, scintillation decay time, afterglow level, and pulse height spectra. In addition, this study also provides the trend of properties against the Pr concentration of LaPS crystals.

2. Materials and Methods

The synthesis of the Pr-doped LaPS samples was performed in the following order. First, 99.99% purity powders of raw materials, including La_2O_3, SiO_2, and Pr_6O_{11} were weighed and blended using an agate mortar. The Pr-doped concentrations were 0.5, 1.0, 3.0, 5.0, and 10.0 mol% in respect to La, for a total of 5 samples. After blending, cold isostatic pressing was performed for packing the blended powder into a rod shape. All sample rods were sintered by electric furnace at 1400 °C for 10 h. The sintered rods were melted to grow single crystals using a desktop floating-zone furnace (FZD0192, Canon machinery, Canon Machinery Inc., Shiga Prefecture, Japan). In this machine, the heat is generated by dual halogen lamps with a pulling-down rate of 5 mm/h. After the crystal growth was successful, the obtained single crystal rods were cut and polished to a suitable size for characterization. The phase confirmation of the synthesized Pr-doped LaPS was performed via powder X-ray diffraction (XRD) analysis (MiniFlex600, Rigaku, Tokyo, Japan). The sample powder used in XRD measurement was ground crystals of the remaining small pieces after the cutting process. In addition, the polished samples were used for a density measurement by Archimedes' principle and a diffused transmittance measurement by spectrophotometer (SolidSpec-3700, Shimadzu, Kyoto, Japan).

The characterization of Pr-doped LaPS was divided into two parts, the PL properties and the scintillation properties. In the first part of the characterization of PL properties, PL emission and excitation were combined to the PL emission contour map, which was measured by the quantum yield spectrometer (Quantaurus-QY C11347-01, Hamamatsu Photonics, Shizuoka, Japan). The excitation and the observation wavelength were 250–500 and 260–700 nm, respectively. Along with PL emission properties, the PL decay time analysis was performed with a fluorescence lifetime spectrometer (Quantaurus-Tau C11367, Hamamatsu photonics). The selection of the emission was based on the information from the emission and excitation contour graph mentioned above. In this compound, the Pr^{3+} 5d–4f transition was attractive in scintillator uses so the emission due to this transition was focused. The spectrometer internal LED with a 280 nm wavelength was selected as an excitation source. The observation wavelength was 330 nm with an adequate bandpass filter (MZ0340, Asahi Spectra, Tokyo, Japan). The time range of the PL decay time measurement was 200 ns.

The second part involved scintillation properties. The X-ray-induced scintillation spectra were evaluated by using our in-house developed instruments [28]. The sample was attached to the fiber optic that led to the CCD spectrometer (DU-420-BU2, Andor Technology, Belfast, Northern Ireland). In this measurement, the total X-ray dose was 1 Gy and the observation wavelength was 200–700 nm. The X-ray-induced scintillation decay time and afterglow measurements were also performed by our in-house setup [29]. The scintillation decay time measurement had an observation wavelength of 160–650 nm with a time range of 1 μs. On the other hand, the afterglow analysis in this study was focused on the afterglow level at 20 ms after X-ray irradiation (Af_{20}). The final scintillation

property was the pulse-height spectrum, characterized by our original instruments [30]. The ^{137}Cs was selected as a 662 keV γ-ray source. In this measurement, a photomultiplier tube (R7600-200, Hamamatsu Photonics) was used as a photodetector, and the shaping time of a shaping amplifier (572, ORTEC, Oak Ridge, TN, USA) was adjusted to 2 μs. The Pr-doped LPS from our previous study was used as a reference sample with a scintillation light yield of 9700 ph/MeV [31]. Since the Pr-doped LPS and Pr-doped LaPS had the same scintillation wavelength, the scintillation light yield was calculated by this equation.

$$LY_s = LY_R \times (N_S/N_R) \quad (1)$$

In Equation (1), LY_s is the light yield of target sample's, LY_R is that of the reference one, N_s is the photoabsorption peak channel number of the target sample, and N_R is that of the reference one. In addition, the energy resolution of the highest scintillation light yield sample was calculated by this equation under the approximation of a single Gaussian function.

$$\Delta E = 2.35\ (\sigma/P_g) \times 100\% \quad (2)$$

In Equation (2), ΔE is energy resolution, σ is the photoabsorption's width, and P_g is the Gaussian peak.

3. Results and Discussion

3.1. Sample Conditions

Figure 1a presents a photograph of the obtained 10% Pr-doped LaPS single crystal rod after the crystal growth process. All the sample rods had a diameter of 5 mm with a 30–35 mm length accompanied by some internal cracks, as shown in Figure 1a. When comparing the as-grown rod with the sintered part, the appearance was obviously different. In addition, the colors of samples with low Pr concentration were transparent and colorless. The color of the samples gradually became more yellow-green following the rising of Pr-doped concentration in each LaPS sample. This trend is clearly shown in the cut and polished samples in Figure 1b. The thickness of the polished samples was 1 mm.

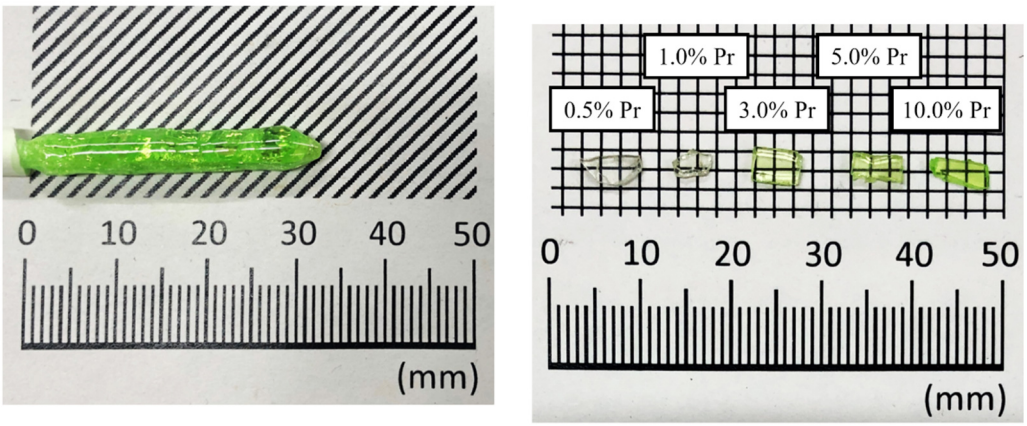

(**a**) (**b**)

Figure 1. Photographs of Pr-doped LaPS single crystal samples: (**a**) as-grown (10.0% Pr-doped); (**b**) after being cut and polished.

After the cut and polish, some remaining portions of the grown crystals were crushed to a powder for XRD measurement. Figure 2 presents the XRD patterns of the Pr-doped LaPS samples. The obtained XRD patterns of the samples were matched with the JCPDS 82-0729 reference pattern (monoclinic $La_2Si_2O_7$). In addition, the other phases in the La_2O_3-SiO_2 quasi-binary system, including La_2SiO_5 and $7La_2O_3 \cdot 9SiO_2$, were undetectable by our X-ray diffractometer [32].

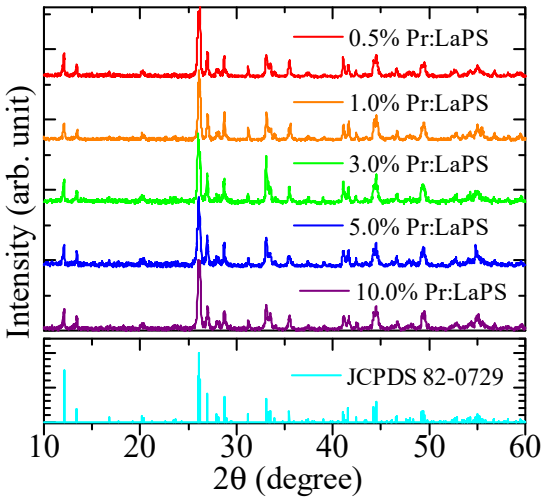

Figure 2. XRD patterns of Pr-doped LaPS samples with the JCPDS 82-0729 reference pattern ($La_2Si_2O_7$).

Figure 3 shows the transmittance spectra of Pr-doped LaPS samples. Every sample had two absorption bands at 450–500 nm and 600 nm, respectively, due to the Pr^{3+} 4f–4f transition. Additional discussion occurs in the later PL properties section since 450–500 nm bands were also observed in the excitation spectrum. These absorptions were also related to the yellow-green color that appeared on the high-Pr concentration samples and were relatively colorless in the low-Pr concentration samples as shown in the polished sample in Figure 1b. The high transparency of all the samples is also shown here since the transmittance at the other wavelengths was around 80%.

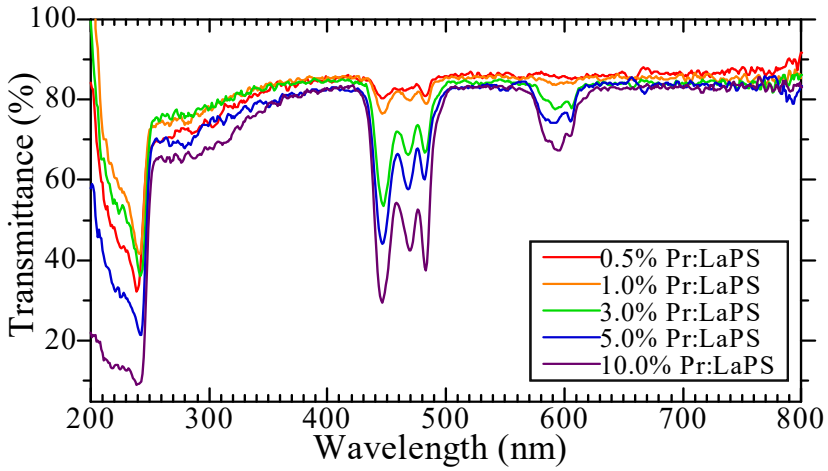

Figure 3. Transmittance spectra of Pr-doped LaPS samples.

3.2. PL Properties

Figure 4 represents PL excitation and emission contour maps of the 3.0% Pr-doped LaPS sample as a representative. The other Pr-doped LaPS samples had similar PL excitation and emission bands to 3.0% Pr-doped LaPS sample. The 3.0% Pr-doped LaPS samplehad four emission bands. Under the 250 nm excitation, the first emission band at 280–310 nm was ascribed to the 5d–4f transitions of Pr^{3+}. This emission was also focused on later PL decay time analysis. Under the 300–340 nm excitation, the second emission band at 360–390 nm was ascribed to the host emission. For this emission band, the supporting evidence and discussion are provided in the later scintillation spectra results section. Under the 430–490 nm excitation, the third band at 490–500 nm and the fourth emission band at 600–660 nm were ascribed to Pr^{3+} 4f–4f transitions of $^3H_4 \rightarrow {}^3P_0$ and $^3H_4 \rightarrow {}^1D_2$, respectively [33].

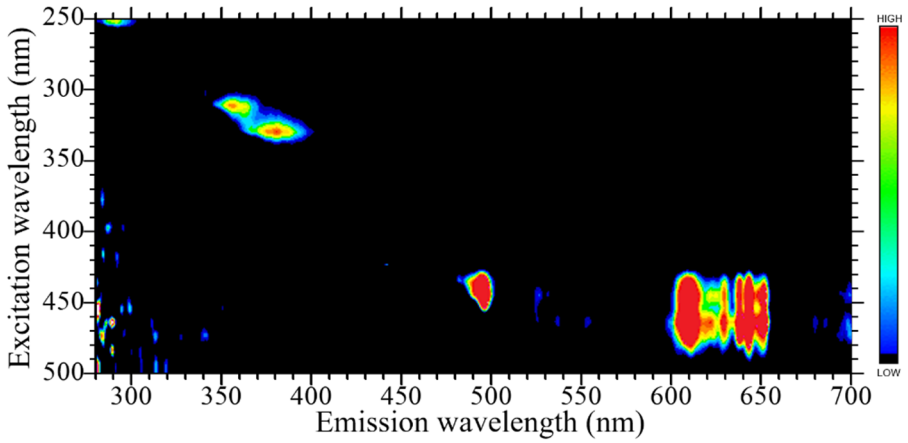

Figure 4. PL emission contour map of the 3.0% Pr-doped LaPS sample. The horizontal and vertical axes show emission and excitation wavelengths, respectively.

In Figure 5, PL decay time profiles of Pr-doped LaPS are presented. As explained above, we now focus on the emission from 5d–4f transitions of Pr^{3+}. The PL decay curves of Pr-LaPS are approximated by a single exponential function. In addition, the approximate formula does not include the initial part of the decay curve since it is affected by the instrument response function (IRF). The PL decay time constants of Pr-doped LaPS were around 18–19 ns. This decay constant originated from 5d–4f transitions of Pr^{3+}, consistent with the other Pr-doped materials [34].

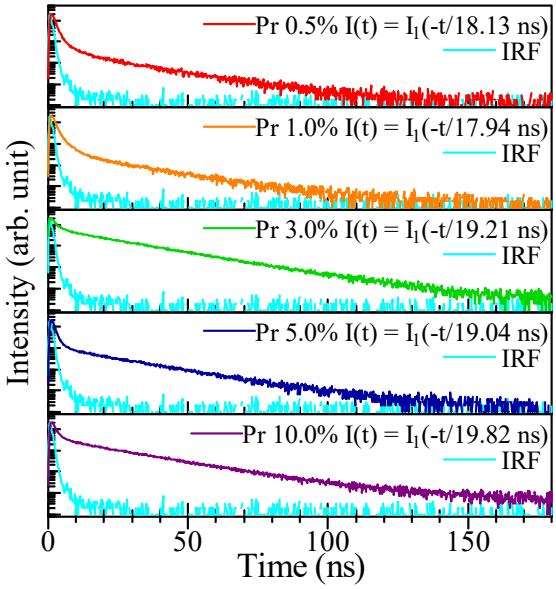

Figure 5. PL decay time profile of Pr-doped LaPS samples. The excitation and emission wavelengths are 280 and 330 nm, respectively.

3.3. Scintillation Properties

Figure 6 shows X-ray-induced scintillation spectra of the Pr-doped LaPS and undoped LaPS as a reference. The intensity in this measurement only represents a qualitative value, and only the emission wavelength should be focused upon. The scintillation light yields comparison is dicussed later in the pulse hight spectra. Every Pr-doped LaPS sample had a similar spectral shape. In addition, the scintillation spectra also contained similar emissions to the previously discussed PL emission map. The origin of each emission band is explained as follows. The first couple of intense peaks at 250–300 nm come from the Pr^{3+} 5d–4f transition. This emission also appeared in the Pr-doped LPS and LuAG

spectra [24,35]. When comparing the Pr-doped LaPS to the undoped one, the scintillation band between 350–400 nm appeared on both samples. Thus, this emission could come from the LaPS host, and the possible origin would be the self-trapped exciton (STE). Detection of a similar emission band in undoped YPS, GPS, and LPS also support this interpretation [36]. Finally, the two sharp scintillation groups at 480–500 and 600–650 nm originated from the Pr^{3+} 4f–4f transitions $^3H_4 \rightarrow {}^3P_0$ and $^3H_4 \rightarrow {}^1D_2$, respectively [33,37].

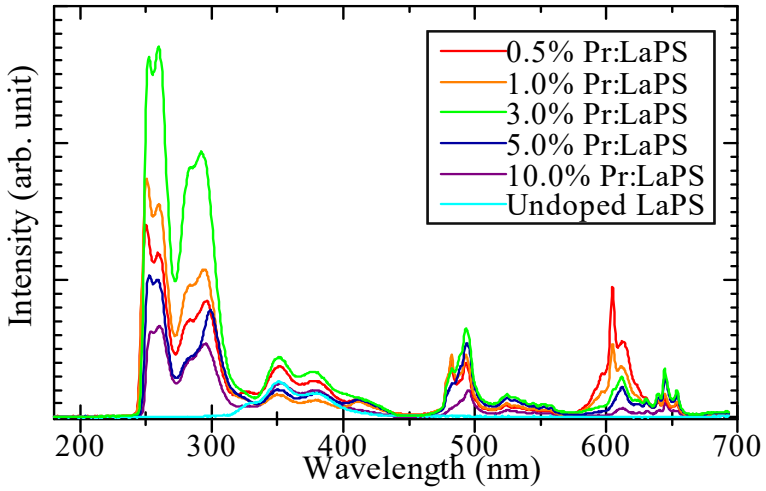

Figure 6. X-ray-induced scintillation spectra of the Pr-doped LaPS and the undoped LaPS.

The X-ray-induced scintillation decay time profiles of the Pr-doped LaPS samples and approximation formula of each sample are presented in Figure 7. The decay time profile of each sample was approximated with a sum of two exponential functions. The first decay constant was attributed to the Pr^{3+} 5d–4f transition, which is the dominant component in this profile (96.4 to 4.6%). The first decay time constant between 25–27 ns is typical for the scintillation of Pr^{3+} 5d–4f transitions in the pyrosilicate host [25]. On the other hand, the origin of the second decay time component is not clear. One of the possibilities is the STE that appeared on previous scintillation spectra. When comparing the Pr-doped LaPS to the other famous oxide scintillator, Pr-doped LaPS have a significantly faster scintillation decay time than the Ce-doped Lu_2SiO_5 (LSO, 40 ns) [38] and Gd_2SiO_5 (GSO, 56 ns) [39].

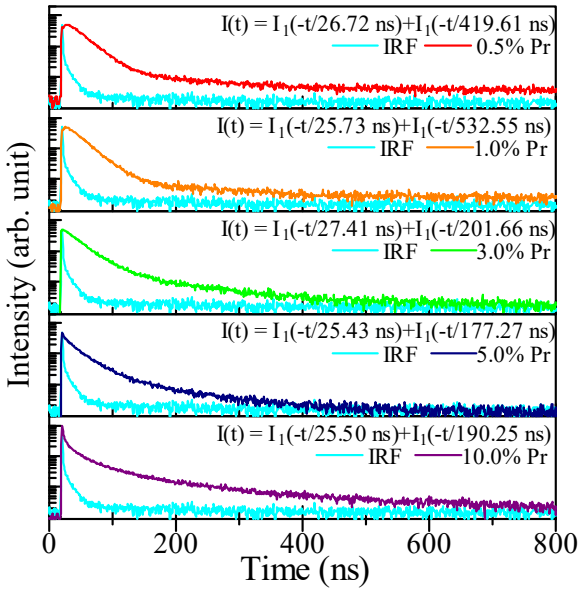

Figure 7. X-ray-induced scintillation decay time profile of the Pr-doped LaPS samples.

Figure 8 presents the afterglow time profiles of Pr-doped LaPS samples with the Af_{20}. The lowest Af_{20} in this study can be found in the 3.0% Pr-doped LaPS sample at 34 ppm. In addition, the afterglow levels of Pr-doped LaPS samples are considerably low when compared with the Af_{20} of some commercial scintillators on the market such as $CdWO_4$ (140 ppm) and Tl-doped CsI (268 ppm) [40,41].

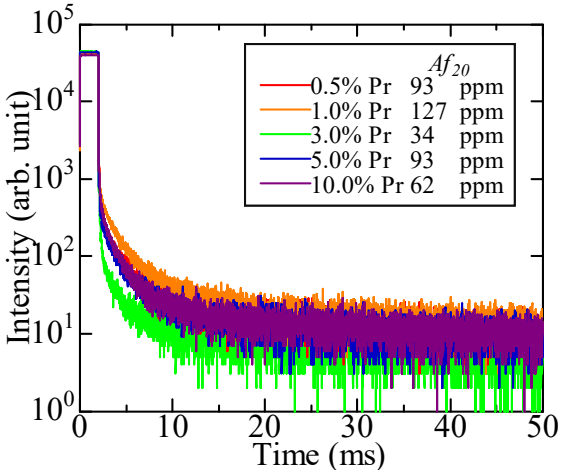

Figure 8. Afterglow time profile of Pr-doped LaPS samples.

Figure 9a shows the pulse-height spectra of Pr-doped LaPS samples with the Pr-doped LPS under 662 keV γ-ray irradiation from ^{137}Cs. The channel of the photoabsorption peak of each Pr-doped LaPS sample and the 1.0% Pr-doped LPS as a reference were used to calculate the absolute scintillation light yield. The calculation results against Pr-doped concentration are presented in Figure 9b. The trends of the optimum Pr-doped concentration for scintillation are observed. The highest scintillation light yield in this study is 3200 ph/MeV from the 3.0% Pr-doped LaPS sample. In addition, the energy resolution of the 3.0% Pr-doped LaPS is 15.5%, which improved from 19.8% of 1.0% Pr-doped LPS. However, the improvement of the energy resolution of Pr-LaPS is possible by changing the synthesized method to the Czochralski method to improve the overall crystal quality. Finally, after all of the characterizations, Table 1 summarizes the properties of Pr-doped LaPS.

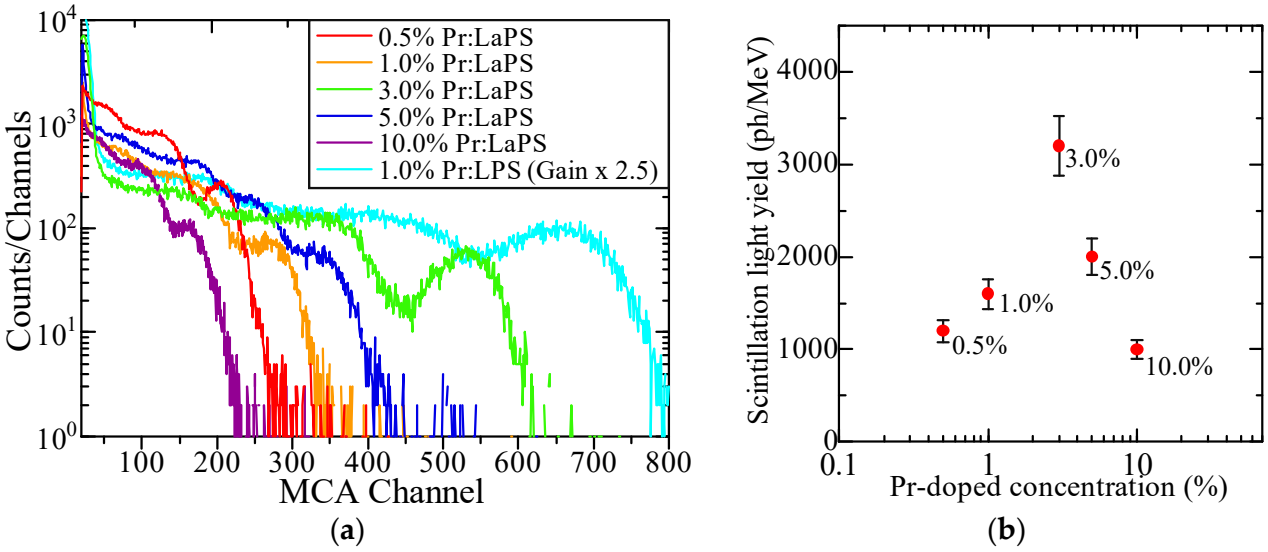

Figure 9. ^{137}Cs, 662 eV γ-ray: (**a**) pulse-height spectra of Pr-doped LaPS samples with the Pr-doped LPS spectrum; (**b**) scintillation light yield of LaPS samples plotted against Pr concentration.

Table 1. Pr-doped LaPS summarized data.

Sample	Density (g/cm^3)	Z_{eff}	PL Emission Wavelength (nm)	PL Decay Time (ns)	Scintillation Wavelength (nm)	Scintillation Decay Time (ns)	Af_{20} (ppm)	662 keV γ-ray Scintillation Light Yield (ph/MeV)
0.5% Pr-doped LaPS	4.64	50.6	280–310 (5d–4f), 350–400 (STE), 490–500 + 600–660 (4f–4f)	18.1	250–310 (5d–4f), 350–400 (STE), 480–500 + 600–650 (4f–4f)	26.7, 419.6	93	1200
1.0% Pr-doped LaPS	4.56			17.9		25.7, 532.5	127	1600
3.0% Pr-doped LaPS	4.43			19.2		27.4, 201.6	34	3200
5.0% Pr-doped LaPS	4.68			19.0		25.4, 177.2	93	2000
10.0% Pr-doped LaPS	4.74			19.8		25.5, 190.2	62	1000

4. Conclusions

The LaPS single crystals with a Pr-doping concentration of 0.5–10.0% were successfully grown by the floating zone method with the phase confirmation from the XRD pattern matched with the reference. The optical and scintillation properties of Pr-doped LaPS single crystals were evaluated in this study for the first time. In the PL emission and X-ray-induced scintillation spectra, Pr-doped LaPS exhibited multiple emissions, including the Pr^{3+} 5d–4f transition at 250–310 nm, which is a preferable emission for scintillator usage. This emission had a PL and scintillation decay time of around 19 and 26 ns, respectively. Under ^{137}Cs 662 keV γ-ray irradiation, the 3.0% Pr-doped LaPS had a scintillation light yield of up to 3200 ph/MeV, which was the best value among the present samples. The lowest afterglow level of the Pr-doped samples was 34 ppm, which is considerably low when compared with most commercially available scintillators. In addition, Table 1 presents all of the relevant properties observed in this study. When considering all of the properties in this study, the optimal Pr concentration in LaPS is 3.0 mol% for scintillator usage. Overall, Pr-doped LaPS is an interesting candidate for a fast decay scintillator for a specific need such as nuclear medical imaging. However, further study on the temperature dependence properties and radiation tolerance are required for a better understanding of the behavior of this crystal as a scintillation detector. Different synthesis methods to grow a Pr-doped LaPS single crystal with a higher crystal quality would also be interesting for the improvement of scintillation light yield as well as energy resolution.

Author Contributions: Conceptualization, P.K.; methodology, P.K. and T.Y.; validation, T.K., D.N. and N.K.; formal analysis, P.K. and T.Y.; investigation, P.K. and T.Y.; resources, T.Y.; data curation, P.K.; writing—original draft preparation, P.K.; writing—review and editing, P.K. and T.Y.; visualization, P.K.; supervision, T.Y.; funding acquisition, T.K., D.N., N.K. and T.Y. All authors have read and agreed to the published version of the manuscript.

Funding: This work was supported by the Cooperative Research Project of the Research Center for Biomedical Engineering, Nippon Sheet Glass Foundation, Nara Institute of Science and Technology (NAIST) special fund, and Iketani Science and Technology. In addition, the Japan Society for the Promotion of Science (JSPS) is also acknowledged for Grant-in-Aid for Scientific Research B (19H03533, 21H03733, and 21H03736) and Early-Career Scientists (20K20104).

Institutional Review Board Statement: Not applicable.

Informed Consent Statement: Not applicable.

Data Availability Statement: Data of the results presented in this article are not publicly available.

Conflicts of Interest: The authors declare no conflict of interest.

References

1. Yanagida, T. Study of rare-earth-doped scintillators. *Opt. Mater.* **2013**, *35*, 1987–1992. [CrossRef]
2. Van Eijk, C.W.E. Inorganic-scintillator development. *Nucl. Instrum. Methods Phys. Res. A* **2001**, *460*, 1–14. [CrossRef]

3. Koshimizu, M.; Yanagida, T.; Kamishima, R.; Fujimoto, Y.; Asai, K. Scintillation Properties and α-ray Detection Capabilities of Thin-film Plastic Scintillators. *Sens. Mater.* **2019**, *31*, 1233. [CrossRef]
4. Takashima, D.; Ozaki, K.; Nishimura, M.; Okada, N.; Akai, D.; Ishida, M. Enhanced Detection Efficiency of Plastic Scintillators upon Incorporation of Zirconia Nanoparticles. *Sens. Mater.* **2015**, *27*, 1. [CrossRef]
5. Masai, H.; Yanagida, T.; Okada, G.; Koreeda, A.; Ohkubo, T. X-ray-induced luminescence of SnO-SrO-B_2O_3 glasses prepared under different preparation conditions. *Sens. Mater.* **2017**, *29*, 1391–1398. [CrossRef]
6. Limkitjaroenporn, P.; Sangwaranatee, N.; Yonphan, S.; Borisut, P.; Kothan, S.; Wongdamnern, N.; Kim, H.J.; Kaewkhao, J. The radioluminescence investigation of lead sodium borate doped with Sm^{3+} glass scintillator. *Radiat. Phys. Chem.* **2022**, *192*, 109887. [CrossRef]
7. Shiratori, D.; Nakauchi, D.; Kato, T.; Kawaguchi, N.; Yanagida, T. X-ray-induced scintillation via energy transfer from Gd^{3+} to Ce^{3+} in silicate glasses composed of heavy elements. *Sens. Mater.* **2020**, *32*, 1365–1372. [CrossRef]
8. Kunikata, T.; Kato, T.; Shiratori, D.; Nakauchi, D.; Kawaguchi, N.; Yanagida, T. Scintillation Properties of Li-doped ZnO Translucent Ceramic. *Sens. Mater.* **2022**, *34*, 661. [CrossRef]
9. Kimura, H.; Kato, T.; Nakauchi, D.; Kawaguchi, N.; Yanagida, T. Radiation-induced luminescence properties of $SrBr_2$ transparent ceramics doped with different eu concentrations. *Sens. Mater.* **2020**, *32*, 1381–1387. [CrossRef]
10. Okazaki, K.; Onoda, D.; Nakauchi, D.; Kawano, N.; Fukushima, H.; Kato, T.; Kawaguchi, N.; Yanagida, T. Scintillation Properties of an Organic–Inorganic Lead Iodide Perovskite Single Crystal Having Quantum Well Structures. *Sens. Mater.* **2022**, *34*, 575. [CrossRef]
11. Onoda, D.; Akatsuka, M.; Kawano, N.; Nakauchi, D.; Kato, T.; Kawaguchi, N.; Yanagida, T. Photoluminescence and scintillation properties of $(C_6H_5C_2H_4NH_3)_2Pb_1-xZnxBr_4$ as a two-dimensional quantum-confined scintillator. *J. Mater. Sci. Mater. Electron.* **2020**, *31*, 20798–20804. [CrossRef]
12. Fukushima, H.; Nakauchi, D.; Kawaguchi, N.; Yanagida, T. Photoluminescence and Scintillation Properties of Ce-doped $SrHfO_3$. *Sens. Mater.* **2019**, *31*, 1273. [CrossRef]
13. Kawaguchi, N.; Kimura, H.; Akatsuka, M.; Okada, G.; Kawano, N.; Fukuda, K.; Yanagida, T. Scintillation characteristics of Pr:CaF2 crystals for charged-particle detection. *Sens. Mater.* **2018**, *30*, 1585–1590. [CrossRef]
14. Akatsuka, M.; Daisuke, N.; Takumi, K.; Kawaguchi, N.; Yanagida, T. Scintillation Properties of Nd-doped $LuVO_4$ Single Crystals. *Sens. Mater.* **2022**, *34*, 619. [CrossRef]
15. McConnell, M.L.; Bloser, P.F.; Legere, J.; Ryan, J.M. Applications for New Scintillator Technologies in Gamma Ray Astronomy. *J. Phys. Conf. Ser.* **2016**, *763*, 012008. [CrossRef]
16. Lesparre, N.; Marteau, J.; Déclais, Y.; Gibert, D.; Carlus, B.; Nicollin, F.; Kergosien, B. Design and operation of a field telescope for cosmic ray geophysical tomography. *Geosci. Instrum. Methods Data Syst.* **2012**, *1*, 33–42. [CrossRef]
17. Glodo, J.; Wang, Y.; Shawgo, R.; Brecher, C.; Hawrami, R.H.; Tower, J.; Shah, K.S. New Developments in Scintillators for Security Applications. *Phys. Procedia* **2017**, *90*, 285–290. [CrossRef]
18. Sanada, Y.; Torii, T. Aerial radiation monitoring around the Fukushima Dai-ichi nuclear power plant using an unmanned helicopter. *J. Environ. Radioact.* **2015**, *139*, 294–299. [CrossRef]
19. Yanagida, T.; Fujimoto, Y.; Kurosawa, S.; Kamada, K.; Takahashi, H.; Fukazawa, Y.; Nikl, M.; Chani, V. Temperature dependence of scintillation properties of bright oxide scintillators for well-logging. *Jpn. J. Appl. Phys.* **2013**, *52*, 3–9. [CrossRef]
20. Melcher, C.L. Scintillation Crystals for PET. *J. Nucl. Med.* **2000**, *41*, 1051–1055.
21. Dujardin, C.; Auffray, E.; Bourret-Courchesne, E.; Dorenbos, P.; Lecoq, P.; Nikl, M.; Vasil'ev, A.N.; Yoshikawa, A.; Zhu, R.-Y. Needs, Trends, and Advances in Inorganic Scintillators. *IEEE Trans. Nucl. Sci.* **2018**, *65*, 1977–1997. [CrossRef]
22. Yanagida, T.; Yoshikawa, A.; Yokota, Y.; Kamada, K.; Usuki, Y.; Yamamoto, S.; Miyake, M.; Baba, M.; Kumagai, K.; Sasaki, K.; et al. Development of Pr:LuAG Scintillator Array and Assembly for Positron Emission Mammography. *IEEE Trans. Nucl. Sci.* **2010**, *57*, 1492–1495. [CrossRef]
23. Pidol, L.; Khan-Harari, A.; Viana, B.; Ferrand, B.; Dorenbos, P.; De Haas, J.T.M.; Van Eijk, C.W.E.; Virey, E. Scintillation properties of $Lu_2Si_2O_7$:Ce3+, a fast and efficient scintillator crystal. *J. Phys. Condens. Matter* **2003**, *15*, 2091–2102. [CrossRef]
24. Kantuptim, P.; Akatsuka, M.; Nakauchi, D.; Kato, T.; Kawaguchi, N.; Yanagida, T. Scintillation properties of Pr-doped $Lu_2Si_2O_7$ single crystal. *Radiat. Meas.* **2020**, *134*, 106320. [CrossRef]
25. Kantuptim, P.; Akatsuka, M.; Kawaguchi, N.; Yanagida, T. Optical and scintillation properties of Pr-doped $Y_2Si_2O_7$ single crystal. *Jpn. J. Appl. Phys.* **2020**, *59*, SCCB17. [CrossRef]
26. Kantuptim, P.; Akatsuka, M.; Nakauchi, D.; Kato, T.; Kawaguchi, N.; Yanagida, T. Scintillation Characteristics of Pr-doped $Gd_2Si_2O_7$ Single Crystal. *Sens. Mater.* **2020**, *32*, 1357–1364. [CrossRef]
27. Kantuptim, P.; Kato, T.; Nakauchi, D.; Kawaguchi, N.; Yanagida, T. Ce concentration dependence of optical and scintillation properties on Ce-doped $La_2Si_2O_7$ crystal. *Jpn. J. Appl. Phys.* **2022**, *61*, SB1038. [CrossRef]
28. Yanagida, T.; Kamada, K.; Fujimoto, Y.; Yagi, H.; Yanagitani, T. Comparative study of ceramic and single crystal Ce:GAGG scintillator. *Opt. Mater.* **2013**, *35*, 2480–2485. [CrossRef]
29. Yanagida, T.; Fujimoto, Y.; Ito, T.; Uchiyama, K.; Mori, K. Development of X-ray-induced afterglow characterization system. *Appl. Phys. Express* **2014**, *7*, 18–21. [CrossRef]
30. Yanagida, T.; Kawaguchi, N.; Fujimoto, Y.; Fukuda, K.; Watanabe, K.; Yamazaki, A.; Uritani, A. Scintillation properties of LiF-SrF2 and LiF-CaF2 eutectic. *J. Lumin.* **2013**, *144*, 212–216. [CrossRef]

31. Yanagida, T.; Watanabe, K.; Okada, G.; Kawaguchi, N. Optical, scintillation and radiation tolerance properties of Pr-doped pyrosilicate crystals. *Jpn. J. Appl. Phys.* **2018**, *57*, 106401. [CrossRef]
32. Kobayashi, K.; Sakka, Y. Rudimental research progress of rare-earth silicate oxyapatites: Their identification as a new compound until discovery of their oxygen ion conductivity. *J. Ceram. Soc. Jpn.* **2014**, *122*, 649–663. [CrossRef]
33. Gorbenko, V.; Zorenko, Y.; Savchyn, V.; Zorenko, T.; Pedan, A.; Shkliarskyi, V. Growth and luminescence properties of Pr3+-doped single crystalline films of garnets and perovskites. *Radiat. Meas.* **2010**, *45*, 461–464. [CrossRef]
34. Nakauchi, D.; Okada, G.; Koshimizu, M.; Yanagida, T. Scintillation and thermally-stimulated luminescence properties of Pr-doped $SrAl_2O_4$ single crystals. *Radiat. Meas.* **2017**, *106*, 170–174. [CrossRef]
35. Yanagida, T.; Fujimoto, Y.; Kamada, K.; Totsuka, D.; Yagi, H.; Yanagitani, T.; Futami, Y.; Yanagida, S.; Kurosawa, S.; Yokota, Y.; et al. Scintillation properties of transparent ceramic pr:LuAG for different pr concentration. *IEEE Trans. Nucl. Sci.* **2012**, *59*, 2146–2151. [CrossRef]
36. Kantuptim, P.; Fukushima, H.; Kimura, H.; Nakauchi, D.; Kato, T.; Koshimizu, M.; Kawaguchi, N.; Yanagida, T. VUV- and X-ray-induced Properties of $Lu_2Si_2O_7$, $Y_2Si_2O_7$, and $Gd_2Si_2O_7$ Single Crystals. *Sens. Mater.* **2021**, *33*, 2195. [CrossRef]
37. Fidelus, J.D.; Yatsunenko, S.; Godlewski, M.; Paszkowicz, W.; Werner-Malento, E.; Łojkowski, W. Relation between structural properties of Pr3+-doped yttria-stabilized zirconia nanopowders and their luminescence efficiency. *Scr. Mater.* **2009**, *61*, 415–418. [CrossRef]
38. Melcher, C.L.; Schweitzer, J.S. A promising new scintillator: Cerium-doped lutetium oxyorthosilicate. *Nucl. Instrum. Methods Phys. Res. A* **1992**, *314*, 212–214. [CrossRef]
39. Takagi, K.; Fukazawa, T. Cerium-activated Gd_2 SiO_5 single crystal scintillator. *Appl. Phys. Lett.* **1983**, *42*, 43–45. [CrossRef]
40. Nagornaya, L.; Onyshchenko, G.; Pirogov, E.; Starzhinskiy, N.; Tupitsyna, I.; Ryzhikov, V.; Galich, Y.; Vostretsov, Y.; Galkin, S.; Voronkin, E. Production of the high-quality $CdWO_4$ single crystals for application in CT and radiometric monitoring. *Nucl. Instrum. Methods Phys. Res. A* **2005**, *537*, 163–167. [CrossRef]
41. Nakauchi, D.; Kato, T.; Kawaguchi, N.; Yanagida, T. Characterization of Eu-doped Ba_2SiO_4, a high light yield scintillator. *Appl. Phys. Express* **2020**, *13*, 2–5. [CrossRef]